GREEN'S FUNCTION MODEL FOR A RECTANGULAR RIJKE TUBE

Patrick R. Murray*[1], Maria A. Heckl[1]

[1] School of Computing and Mathematics, University of Keele
Keele, ST5 5AX, United Kingdom
* Corresponding author: p.r.murray@keele.ac.uk

In an effort to understand and control thermo-acoustic instabilities, we theoretically analyze the stability of a rectangular Rijke tube. This Rijke tube is the generic combustor used in the EU-funded LIMOUSINE project. It is open at both ends, has rectangular cross-section, and is uniform in width so it is described as two dimensional. Our novel approach considers heat sources in the hydrodynamic region. This involves a Green's function approach, where the pressure response from an arbitrary source is calculated by convolution of the source with the Green's function. The Green's function is the wave response to an impulse point source and is calculated using the Schwarz-Christoffel transformation, where the tube geometry is mapped onto the real axis in the transformed space. The transformation has been found numerically and verified by the solution to Laplace's equation for the given geometry. In the long term, we attempt to model the interaction between combustion, acoustics, and aerodynamics in the tube.

1 Introduction

An unsteady heat source within a semi-enclosed body can generate acoustic waves, the amplitudes of which grow due to a thermo-acoustic feedback mechanism which is ultimately unstable. The Rijke tube is the simplest example of one of these bodies. We endeavor to describe the instabilities occurring within the Rijke tube using the Green's function approach.

Previous Green's function solutions for the Rijke tube [1] have assumed the source to be located far downstream of the burner. In this paper, we attempt to describe the Green's function and pressure response originating from a source near to the burner, in a region of the Rijke tube where the flow is disturbed from a one-dimensional state.

We consider the Rijke tube used in the EU-funded LIMOUSINE project. The tube is depicted in Figure 1. It has open ends and has rectangular cross-section. The tube is uniform in width so it is considered two-dimensional. The tube cross-section is in the z-plane and its coordinate axes $\mathbf{x} = (x, y)$ are defined such that the x-axis extends along the length of the tube and the y-axis extends along the height; the origin is located at the center of the tube entrance. The upstream half contains the flame-holder. We model the upstream and downstream regions as having respective cross-sectional area $\mathscr{A}_1$ and $\mathscr{A}_2$, mean temperature $\bar{T}_1$ and $\bar{T}_2$, mean density $\bar{\rho}_1$ and $\bar{\rho}_2$, speed of sound c_1 and c_2, and mean flow u_1 and u_2, where $M_1 = u_1/c_1 \ll 1$ and $M_2 = u_2/c_2 \ll 1$ are the respective Mach numbers. The tube has length L and for our analysis we divide the tube in two three regions: the cold acoustic region, the hydrodynamic region, and the hot acoustic region. The flame region (*hydrodynamic region*) is assumed to be small relative to the wave length of low-order modes so the acoustic motion can be treated as incompressible. X_1 is the interface between the cold acoustic region and the hydrodynamic region and X_2 is similarly the interface between the hydrodynamic region and the hot acoustic region. Interfaces X_1 and X_2 are chosen such that the flow is entirely one-dimensional in $x < X_1$ and $X_2 < x$. The flow is two-dimensional in $X_1 < x < X_2$. We model the temperature and density so that they jump from $\bar{T}_1$, $\bar{\rho}_1$ to $\bar{T}_2$, $\bar{\rho}_2$, respectively, at interface X_2. There are pressure nodes located just outside the tube at locations $x = \ell_1$ and $x = \ell_2$ in order to account for pressure losses at the ends.

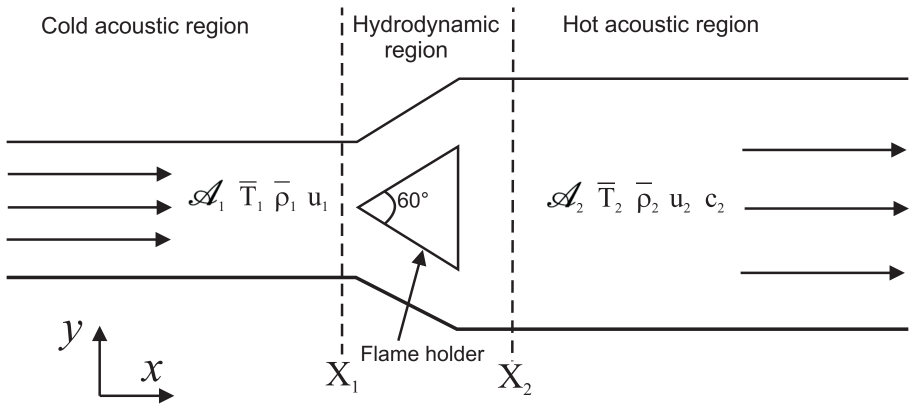

Figure 1: Two-dimensional depiction of Rijke tube

2 The Rijke tube Green's function

The Green's function $G(\mathbf{x}, \mathbf{x}', t-t')$ is the wave response at an observer point $\mathbf{x}$ to an impulse point source located at source position $\mathbf{x}'$ at time $t = t'$ and is a solution of

$$\frac{1}{c^2}\frac{\partial^2 G}{\partial t^2} - \nabla^2 G = \delta(\mathbf{x}-\mathbf{x}')\delta(t-t'), \tag{1}$$

where $c = c(\mathbf{x})$ is the speed of sound at location $\mathbf{x}$, and δ denotes the *Dirac* delta-function. The Green's function is defined to be zero at pressure nodes ℓ_1 and ℓ_2 to account for small pressure transmission at the ends. Eq. (1) assumes the far-field approximation where the distance between the source and the observer $l \gg \lambda$, where λ is the wavelength of the lowest-order mode.

We regard the hydrodynamic region as an airplug oscillating parallel to the x-axis. The conservation equations of mass and momentum across the airplug are respectively

$$\bar{\rho}_1\mathscr{A}_1 u_1 - \bar{\rho}_1\mathscr{A}_2 u_2 = 0, \tag{2}$$

$$p_1 - p_2 = \bar{\rho}_1 L_{eff}\frac{\partial u_1}{\partial t}, \tag{3}$$

where p_1, p_2, $\bar{\rho}_1$, $\bar{\rho}_2$ and u_1, u_2 are the respective pressures, mean densities, and velocities at interfaces X_1 and X_2. L_{eff} designates the effective length of the airplug and is given by the formula (from [1])

$$L_{eff} = \int_{-\infty}^{X_2}\left(\frac{\partial\varphi^*}{\partial x} - 1\right)dx + \int_{X_2}^{\infty}\left(\frac{\partial\varphi^*}{\partial x} - \frac{\mathscr{A}_2}{\mathscr{A}_1}\right)dx + \frac{\mathscr{A}_2}{\mathscr{A}_1}(X_2 - X_1), \tag{4}$$

where $\varphi^*(\mathbf{x})$ is the velocity potential of the hydrodynamic flow in the Rijke tube. Pressure and velocity are continuous across the interfaces X_1 and X_2.

We now consider a Rijke tube with unsteady volume source $q(\mathbf{x}, t)$. We choose to model a volume source rather than a heat source due to its generality; the volume source could model an arbitrary heat source. The velocity potential in the tube ϕ is governed by the acoustic analogy equation

$$\frac{1}{c^2}\frac{\partial^2\phi}{\partial t^2} - \nabla^2\phi = q(\mathbf{x}, t). \tag{5}$$

It's sufficient to assume that waves propagating in the cold and hot acoustic regions are one-dimensional and hence have only x dependence. The flow in the hydrodynamic region remains two-dimensional.

2.1 The time-harmonic Green's function

The time-harmonic Green's function $\hat{G}(\mathbf{x},\mathbf{x}',\omega)$ is found by Fourier transform of the time-domain Green's function

$$\hat{G}(\mathbf{x},\mathbf{x}',\omega) = \int_{-\infty}^{\infty} G(\mathbf{x},\mathbf{x}',t-t')e^{i\omega(t-t')}d(t-t'), \tag{6}$$

where ω is the frequency at which waves propagate.

The time-harmonic Green's function is governed by the Helmholtz equation.

$$\nabla^2\hat{G} + \frac{\omega^2}{c^2}\hat{G} = -\delta(\mathbf{x}-\mathbf{x}'). \tag{7}$$

We assume $\hat{G}$ has the following form in the each of the three regions described in Section 1. We place a source at arbitrary location $\mathbf{x}' = (x', y')$ in the hot acoustic region.

$$\hat{G}(\mathbf{x},\mathbf{x}',\omega) = \begin{cases} a\sin k_1(x-\ell_1) & 0 < x < X_1, \\ \alpha + \beta\varphi^*(\mathbf{x}) & X_1 < x < X_2, \\ ce^{ik_2(x-X_2)} + de^{-ik_2(x-X_2)} & X_2 < x < x', \\ b\sin k_2(x-\ell_2) & x' < x < L, \end{cases} \tag{8}$$

where $k_1 = \omega/c_1$ and $k_2 = \omega/c_2$ are the respective wave numbers in the cold and hot acoustic regions. a, b, c, d, α, and β are unknown coefficients determined using the conservations eqns (2-3) in addition to continuity of pressure and velocity at interfaces X_1 and X_2. $\varphi^*(\mathbf{x})$ is the velocity potential of the hydrodynamic flow in the Rijke tube.

Using eqns (2-3), coefficients c and d are expressed in terms of a. Namely,

$$c = a\gamma, \;\; d = a\gamma^*, \tag{9}$$

where $\cdot^*$ designates the complex conjugate and

$$\gamma(\omega) = \frac{1}{2}\frac{\mathscr{A}_1}{\mathscr{A}_2}\left[\frac{\bar{\rho}_1}{\bar{\rho}_2}\left(\frac{\mathscr{A}_2}{\mathscr{A}_1}\sin\omega\tau_1 + L_{eff}\frac{\omega}{c_1}\cos\omega\tau_1\right) - i\frac{c_2}{c_1}\cos\omega\tau_1\right], \tag{10}$$

where $\tau_1 = (X_1-\ell_1)/c_1$ and $\tau_2 = (X_2-\ell_2)/c_2$ are the times required for sound to travel from an interface, X_1 or X_2, to the corresponding respective pressure node, ℓ_1 or ℓ_2.

Using the *Heaviside* step function $H(\cdot)$, we rewrite $\hat{G}$ so that the entire hot acoustic region is defined by a single expression,

$$\begin{aligned}\hat{G}(\mathbf{x},\mathbf{x}',\omega) \;\; = \;\; & 2aH(x'-x)\left[\Re(\gamma(\omega))\cos k_2(x-X_2) - \Im(\gamma(\omega))\sin k_2(x-X_2)\right] \\ & +bH(x-x')\sin k_2(x-l_2),\end{aligned} \tag{11}$$

where $\Re(\cdot)$ and $\Im(\cdot)$ respectively designate the real and imaginary parts. Substitution in the Helmholtz equation (7) leads to an expression containing coefficients of $\delta(x-x')$ and its derivative $\delta'(x-x')$, yielding the following linear equation a and b:

$$\begin{aligned}-2a\left[\Re(\gamma(\omega))\cos k_2(x'-X_2) - \Im(\gamma(\omega))\sin k_2(x'-X_2)\right] + b\sin k_2(x'-\ell_2) &= 0 \\ 4k_2\left[\Re(\gamma(\omega))\sin k_2(x-X_2) + \Im(\gamma(\omega))\cos k_2(x-X_2)\right] + 2bk_2\cos k_2(x-\ell_2) &= 2\end{aligned} \tag{12}$$

The determinant on the left-hand side of this equation is simplified to give

$$f(\omega) = \frac{1}{2}\frac{\mathscr{A}_1}{\mathscr{A}_2}\left[\frac{\bar{\rho}_1}{\bar{\rho}_2}\cos\omega\tau_2\left(\frac{\mathscr{A}_2}{\mathscr{A}_1}\sin\omega\tau_1 + L_{eff}\frac{\omega}{c_1}\cos\omega\tau_1\right) - \frac{c_2}{c_1}\cos\omega\tau_1\sin\omega\tau_2\right]. \tag{13}$$

The zeros of the function $f(\omega)$ are the eigenfrequencies for the system.

Crammer's rule is used to determine the coefficients a and b:

$$a = \frac{-2\sin\frac{\omega}{c_2}(x'-\ell_2)}{f(\omega)}, \quad b = \frac{-4\left(\Re(\gamma(\omega))\cos\frac{\omega}{c_2}(x'-X_2) - \Im(\gamma(\omega))\sin\frac{\omega}{c_2}(x'-X_2)\right)}{f(\omega)}. \tag{14}$$

Continuity of pressure conserved across the two interfaces X_1 and X_2 is written as

$$\begin{aligned} \bar{\rho}_1\hat{G}_1(X_1,\mathbf{x}',\omega) &= \bar{\rho}_1\hat{G}_2(X_1,\mathbf{x}',\omega) \\ \bar{\rho}_1\hat{G}_2(X_2,\mathbf{x}',\omega) &= \bar{\rho}_2\hat{G}_3(X_2,\mathbf{x}',\omega), \end{aligned} \tag{15}$$

where $\hat{G}_1$, $\hat{G}_2$, and $\hat{G}_3$ are the parts of $\hat{G}(x,x',\omega)$ respectively defined within $0<x<X_1$, $X_1<x<X_2$, and $X_2<x<x'$. Continuity equations (15) are used to determine the coefficients α and β in terms of a:

$$\alpha = a\frac{\sin\omega\tau_1\varphi^*(X_2) - 2\frac{\bar{\rho}_2}{\bar{\rho}_1}\Re(\gamma(\omega))\varphi^*(X_1)}{\varphi^*(X_2)-\varphi^*(X_1)}, \quad \beta = a\frac{2\frac{\bar{\rho}_2}{\bar{\rho}_1}\Re(\gamma(\omega)) - \sin\omega\tau_1}{\varphi^*(X_2)-\varphi^*(X_1)}. \tag{16}$$

Calculations hitherto have assumed a source location in the hot acoustic region. Our novel approach has led to calculations involving observer points located in the hydrodynamic region. Henceforth we employ reciprocity [2] in order to calculate the effect of sources located in hydrodynamic region and observer points at arbitrary position in the tube. Reciprocity states the potential at observer point $\mathbf{x}_A$ due to a source located at point $\mathbf{x}_B$ is equivalent to the potential at observer point $\mathbf{x}_B$ in response to a source at point $\mathbf{x}_A$. Explicitly,

$$\hat{G}(\mathbf{x}_A,\mathbf{x}_B,\omega) = \hat{G}(\mathbf{x}_B,\mathbf{x}_A,\omega) \tag{17}$$

We write the expression for the time-harmonic Green's function corresponding to a source in the hydrodynamic region and observer in the hot acoustic region as

$$\hat{G}(\mathbf{x},\mathbf{x}',\omega) = \frac{-2\hat{g}(\mathbf{x},\mathbf{x}',\omega)}{f(\omega)}, \tag{18}$$

where

$$\hat{g}(\mathbf{x},\mathbf{x}',\omega) = \begin{cases} B(x,\omega)A(x',\omega) & 0<x'<X_1 \\ A(x,\omega)C(\mathbf{x}',\omega) & X_1<x'<X_2 \\ B(x,\omega)D(x',\omega) & X_2<x'<x \\ D(x,\omega)B(x',\omega) & x<x'<L, \end{cases} \tag{19}$$

with

$$A(x,\omega) = \sin\frac{\omega}{c_1}(x-\ell_1) \tag{20}$$

$$B(x,\omega) = \sin\frac{\omega}{c_2}(x-\ell_2) \tag{21}$$

$$C(\mathbf{x},\omega) = \frac{\bar{\rho}_2}{\bar{\rho}_1}\Re(\gamma(\omega))\frac{\varphi^*(\mathbf{x})-\varphi^*(X_1)}{\varphi^*(X_2)-\varphi^*(X_1)} + \sin\omega\tau_1\frac{\varphi^*(X_2)-\varphi^*(\mathbf{x})}{\varphi^*(X_2)-\varphi^*(X_1)} \tag{22}$$

$$D(x,\omega) = \frac{\bar{\rho}_1}{\bar{\rho}_2}\left(\sin\omega\tau_1 + L_{eff}\frac{\mathscr{A}_1}{\mathscr{A}_2}\frac{\omega}{c_1}\cos\omega\tau_1\right)\cos\frac{\omega}{c_1}(x-X_2) + \frac{\mathscr{A}_1}{\mathscr{A}_2}\frac{c_2}{c_1}\cos\omega\tau_1\sin\frac{\omega}{c_2}(x-X_2) \tag{23}$$

In order to calculate the Green's function, velocity potential, and pressure, we must first numerically determine the function $\varphi^*(\mathbf{x})$, which is by best approximation the solution of Laplace's equation within the tube geometry. We choose conformal mapping in order to determine the function because it transforms a complex geometry with several angles into the much simpler real axis in the complex plane.

2.2 Calculation of φ^*

When describing the conformal mapping of the Rijke tube, we change notation in order to avoid confusion. We no longer use vector notation $\mathbf{x} = (x, y)$ and instead use complex notation $z = x + iy$. Correspondingly, the transformation exists in the complex plane $\zeta = \xi + i\eta$.

The interior of straight-sided polygon in the z-plane can be mapped into the transformed space on the upper half ζ-plane, such that the sides of the polygon are transformed into the real ζ-axis by means of the formula (from [3]):

$$\frac{dz}{d\zeta} = K \prod_{n=1}^{N} (\zeta - \xi_n)^{\alpha_n/\pi - 1} \tag{24}$$

for a polygon with N angular points, where α_n and ξ_n ($\xi_n < \xi_{n+1}$) are the respective internal angles and points on the real ζ-axis ($\zeta_n = \xi_n + i\eta_n$) corresponding to the angular points $z_n = x_n + iy_n$ in the z-plane. K is a complex constant and determines orientation and size. A transformation containing four angular points is depicted in Figure 2. The perimeter of the polygon maps onto the real ζ-axis so that one of the points ξ_n has location $\zeta = \infty$; in this case, the factor $(\zeta - \xi_n)^{\alpha_n/\pi - 1}$ is omitted from the right-hand side of eqn (24).

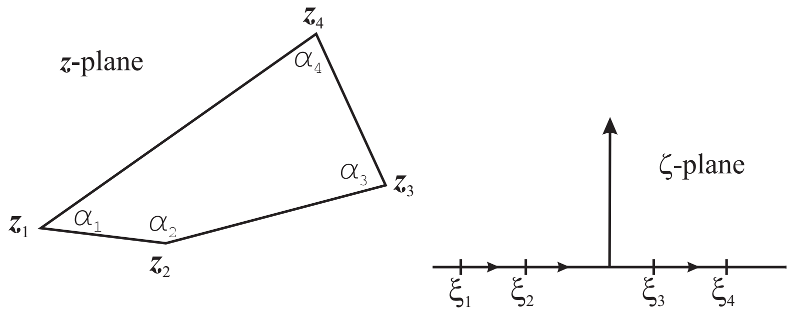

Figure 2: Illustration of Schwarz-Christoffel transformation for an arbitrary polygon

The integral form of eqn (24),

$$z(\zeta) = K \int_{\zeta=\xi} \prod_{n=1}^{N} (\zeta' - \xi_n)^{\alpha_n/\pi - 1} d\zeta' + L, \tag{25}$$

introduces an integration constant L, which determines the position of the polygon in the z-plane. In any transformation, three ξ_n parameters may be prescribed arbitrarily, obeying the condition $\xi_i < \xi_{i+1}$.

2.2.1 Application to the Rijke tube

The Rijke tube in the z-plane is mapped onto the upper half ζ-plane, such that the sides of the tube are transformed to the real ζ-axis using eqn (24). We utilize the apparent symmetry and only discuss the upper-half portion of the tube. The upper-half Rijke tube and its transformation into the ζ-plane are depicted in Figure 3. For the Rijke tube, eqn (24) simplifies to

$$\frac{dz}{d\zeta} = K \frac{(\zeta - \xi_3)^{1/3} (\zeta - \xi_6)^{5/6}}{(\zeta - \xi_2)^{1/3} (\zeta - \xi_4)(\zeta - \xi_5)^{1/3} (\zeta - \xi_7)^{1/2}}. \tag{26}$$

Constants ξ_4 and ξ_5 are chosen to be 0 and 1, respectively. The integral form of eqn (26) is

$$z(\zeta) = K \int_{\zeta} F(\zeta') d\zeta' = K \int_{\zeta} \frac{(\zeta' - \xi_3)^{1/3} (\zeta' - \xi_6)^{5/6}}{\zeta' (\zeta' - \xi_2)^{1/3} (\zeta' - 1)^{1/3} (\zeta' - \xi_7)^{1/2}} d\zeta', \tag{27}$$

where the function on the right-hand side of eqn (26) is defined as $F(\zeta)$. The four unknowns in eqn (27) cannot be determined analytically because the number of parameters ξ_i involved exceeds three. Refer-

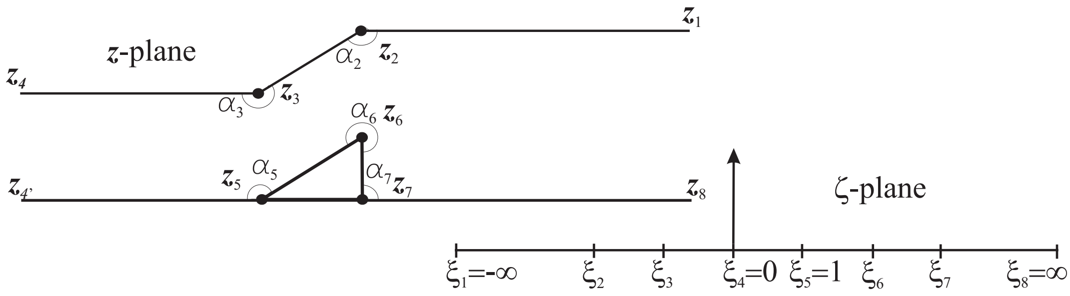

Figure 3: Illustration of Rijke tube transformation from the z plane to the ζ plane

ences [4] and [5] present a numerical method for calculating the constants in the Schwarz-Christoffel transformation of a polygon. The method consists of defining an error S as the sum of the squares of the differences between the ζ-plane integrals and the z-plane displacements for two consecutive points. Specifically,

$$S = \sum_{n=1}^{N-1} \left| K \int_{\zeta=\xi_n}^{\zeta=\xi_{n+1}} F(\zeta')d\zeta' - (z_{n+1} - z_n) \right|^2 , \tag{28}$$

for all n corresponding to ξ_n having finite position in the ζ-plane, where N is the total number of points. The error should tend toward zero; however, it cannot be exactly zero due to the numerical nature so we search for error $S < 10^{-6}$.

It is essential when calculating the error to devise a well-behaved numerical integration scheme due to the singular nature of $F(\zeta)$. For example, if integrating between ξ_3 and ξ_4 in eqn (27), a zero would be encountered at ξ_3 and a first-order pole would be encountered at ξ_4.

Given the Schwarz-Christoffel transformation is defined such that $\xi_i < \xi_{i+1}$, singularities and zeros exist only at the limits of integration, not between them. The Gauss-Jacobi quadrature addresses this problem. [6] approximates an integral having a singular integrand using Gaussian integration. Namely,

$$\int_{-1}^{1} (1+x)^{\beta}(1-x)^{\gamma} f(x)dx \simeq \sum_{j=1}^{M} W_j f(x_j), \tag{29}$$

where M is the chosen number of abscissae x_i and weights W_i.

2.2.2 Minimization of the error

When a function is continuous and smooth, we employ a simple method of convergence, like Newton-Raphson, which is gradient-dependent. However, when calculating the Schwarz-Christoffel transformation, the gradient is not practical to calculate because it is either highly singular or zero at the points of interest. It is therefore essential to employ a convergence scheme in which the gradients are not necessary.

The chosen method of convergence is called the *simplex* method. A simplex is the N-dimensional analogue to a triangle containing $N+1$ independent points in euclidean space, N being the number of dimensions in the function.

For the Rijke tube transformation, the simplex is initiated at step $P = 1$ with $N+1$ arbitrary points at $\left\{\mathbf{X}_{n=n_1}, \mathbf{X}_{n=n_2}, ..., \mathbf{X}_{n=N+1}\right\}$, it then replaces the point having the largest error $S\left(\mathbf{X}_{n=n_j}^{P=1}\right)$ with the dimensionally-*opposite* point. If in the following step $P = 2$, the dimensionally-opposite point $\mathbf{X}_{n=n_j}^{P=2}$ corresponds to an error S which is smaller than in the previous step, the procedure will do either one of the following. If the error at a different point in the simplex $S\left(\mathbf{X}_{n\neq n_j}^{P=2}\right)$ is greater than $S\left(\mathbf{X}_{n=n_j}^{P=2}\right)$, $\mathbf{X}_{n\neq n_j}^{P=2}$ is replaced with the dimensionally-opposite point $\mathbf{X}_{n\neq n_j}^{P=3}$ in the following step; however, if $S\left(\mathbf{X}_{n=n_j}^{P=2}\right)$ is still greater than the error at any other point, the simplex expands in the direction between $\mathbf{X}_{n=n_j}^{P=1}$ and $\mathbf{X}_{n=n_j}^{P=2}$. If replacement leads to an error which is smaller than any other, the simplex contracts. This procedure continues for several iterations until converging upon the minimum, in this case $S < 10^{-6}$. The chosen method of convergence is described in [7], Chapter 10.

2.2.3 *Hydrodynamic streamlines*

In order to validate the determined parameters of the Schwarz-Christoffel transformation, we calculate the streamlines of the potential flow originating from a source at negative infinity in the z-plane. The complex potential w is defined as $\varphi + i\psi$, where φ is the velocity potential and ψ is the streamline value. Transformation into the z-plane is performed by integrating the function $dz/d\zeta$ between the ζ value chosen to correspond to $z = 0$, $\zeta_{z=0}$, and ζ, where

$$\zeta = \pm\sqrt{\mathrm{e}^{\pi\varphi/q_o}\left(\cos\left(\frac{\pi\psi}{q_o}\right) + i\sin\left(\frac{\pi\psi}{q_o}\right)\right)} \tag{30}$$

The ζ-plane source configuration corresponding to eqn (30) is depicted in Fig. 4

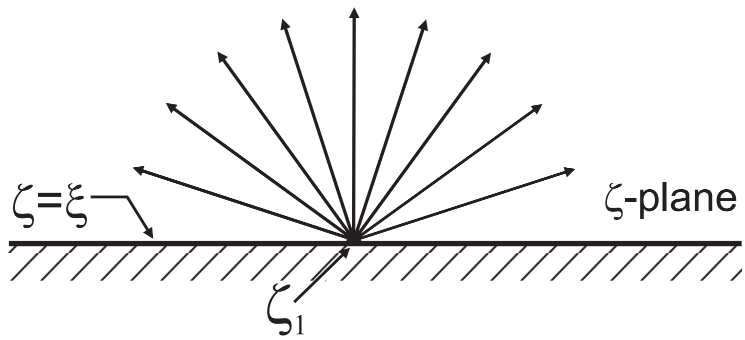

Figure 4: A point source and its image about an infinite plane at $\zeta = \xi$.

The streamlines are calculated allowing $\varphi/\mathscr{A}_1$ to vary over the range $(-\infty, \infty)$ for fixed values of ψ in the range $0 \le \psi/\mathscr{A}_1 \le 1$, where $\psi/\mathscr{A}_1 = 0$ and $\psi/\mathscr{A}_1 = 1$ respectively correspond to the lower boundary (centerline of the Rijke tube) and upper boundary of the geometry.

Numerical results have been obtained for the Schwarz-Christoffel transformation of the Rijke tube. The minimization procedure requires $P \sim 500$ steps. The functional form of the transformation is

$$z(\zeta) = K\int_a^{\zeta} \frac{(\zeta' + 1.309)^{1/6}(\zeta' - 586.4)^{2/3}}{\zeta'(\zeta + 393.1)^{1/6}(\zeta - 1)^{1/6}(\zeta - 2720)^{1/2}}, \text{ where } K = 8.04,\ a = 1. \tag{31}$$

The calculated streamlines are depicted in Fig. 5. The streamlines obtained using the Schwarz-Christoffel transformation are identical to those obtained using numerical integration of Laplace's equation which validates the transformation. We use the numerical values of $\varphi^*(\mathbf{x})$ in order to calculate the Green's function.

2.3 The time-domain Green's function

We calculate the time-domain Green's function $G(\mathbf{x}, \mathbf{x}', t - t')$ from the time-harmonic Green's function by inverse Fourier transform,

$$G(\mathbf{x}, \mathbf{x}', t - t') = -\frac{1}{2\pi}\int_{-\infty}^{\infty} \hat{G}(\mathbf{x}, \mathbf{x}', \omega)e^{-i\omega(t-t')}d\omega. \tag{32}$$

The integration path is the contour which extends the entire real ω-axis and passes through the negative ω-plane, enclosing all singularities occurring at the eigenfrequencies $f(\omega_n) = 0$. The transform is

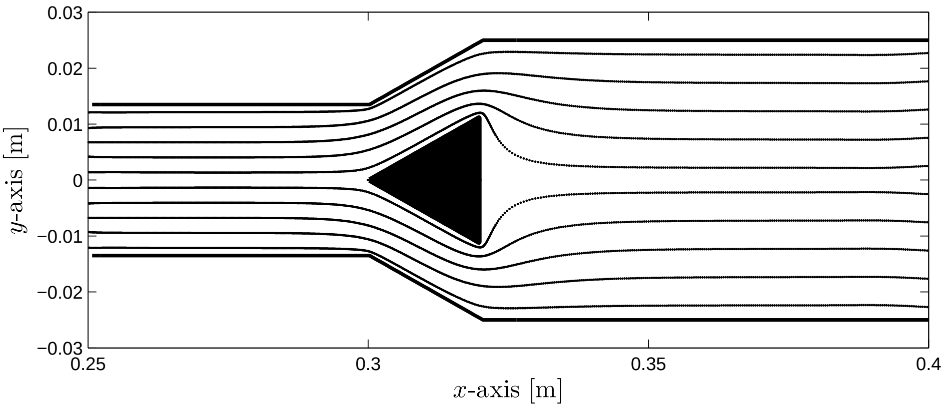

Figure 5: Streamlines of the incompressible, irrotational flow in the chosen Rijke tube

calculated using the method of residues. The function $\hat{g}(\mathbf{x},\mathbf{x}',\omega)$ in Eq. (18) has two properties which simplify the transform equation. The residue vanishes at the trivial eigenfrequency $\omega = \omega_0 = 0$. Also, the function $\hat{g}(\mathbf{x},\mathbf{x}',\omega)$ exhibits symmetry where $-\omega_n = \omega_{-n}$. For each Rijke tube eigenfrequency ω_n there exists a singularity of order one. The Green's function is found to be

$$G(\mathbf{x},\mathbf{x}',t-t') = 2H(t-t')\sum_{n=1}^{\infty}\frac{\hat{g}(\mathbf{x},\mathbf{x}',\omega_n)}{f'(\omega_n)}\sin\omega_n(t-t'). \tag{33}$$

We introduce the Heaviside function $H(t-t')$ in order to ensure causality.

3 Response to a point source in the hydrodynamic region

There are several quantities of interest which we can obtain from the Green's function including the velocity potential ϕ and the unsteady pressure $p = -\rho\frac{\partial\phi}{\partial t}$. The velocity potential is found by convolution of the Green's function with the source [8],

$$\phi(\mathbf{x},t) = \int\int_{-\infty}^{\infty} G(\mathbf{x},\mathbf{x}',t,t')q(\mathbf{x}',t')d\mathbf{x}'dt'. \tag{34}$$

We illustrate the effect of two source configurations, each located in the hydrodynamic region. The first source configuration (i) consists of a volume source of strength q_o with fixed location just downstream of the burner at $\mathbf{x}_q$. The source amplitude oscillates at a chosen Rijke tube eigenfrequency ω_q. The source function is

$$q(\mathbf{x},t) = q_o\delta(\mathbf{x}-\mathbf{x}_q)\cos\omega_q t. \tag{35}$$

The expression for the observed pressure is calculated using eqn (32) and eqn (34). We integrate over space, time, and frequency, in that order. The exact expression for the pressure is

$$p(\mathbf{x},t) = q_o\rho_2\omega_q\cos w_q t\frac{\hat{g}(\mathbf{x},\mathbf{x}_q,\omega_q)}{f(\omega_q)} \tag{36}$$

The second source configuration (ii) is similar to the first except it oscillates in the axial direction about position $\mathbf{x}_q$ at frequency $\omega_{q'}$ over the range $\{\mathbf{x}_q-\mathbf{a},\mathbf{x}_q+\mathbf{a}\}$, where $\mathbf{a}$ is a vector in the axial direction. The source function is

$$q(\mathbf{x},t) = q_o\delta(\mathbf{x}-\mathbf{x}_q-\mathbf{a}\sin\omega_{q'}t)\cos\omega_q t. \tag{37}$$

The expression for the observed pressure is similar to the first except there is a small correction due to the oscillations. The dominating frequency remains ω_q. The expression for the pressure is

$$\begin{aligned} p(\mathbf{x},t) \quad = \quad & \frac{q_o\rho_2}{f(\omega_q)}\Big\{\omega_q\cos\omega_q t\,\hat{g}(\mathbf{x},\mathbf{x}_q,\omega_q) + \frac{|\mathbf{a}|\varphi^{*\prime}(\mathbf{a}\sin\omega_{q'}t+\mathbf{x}_q)}{\varphi^*(X_2)-\varphi^*(X_1)} \\ & \Big[(\omega_q+\omega_{q'})\cos(\omega_q+\omega_{q'})t\Big(\sin(\omega_q+\omega_{q'})\tau_1-\frac{\bar{\rho}_2}{\bar{\rho}_1}\Re(\gamma(\omega_q+\omega_{q'}))\Big) \\ & -(|\omega_q-\omega_{q'}|)\cos(|\omega_q-\omega_{q'}|)t\Big(\sin(|\omega_q-\omega_{q'}|)\tau_1-\frac{\bar{\rho}_2}{\bar{\rho}_1}\Re(\gamma(|\omega_q-\omega_{q'}|))\Big)\Big]\Big\} \end{aligned} \tag{38}$$

where $\varphi^{*\prime}$ designates $\partial\varphi^*/\partial x$. The two source configurations are depicted in Fig. 6. Numerical results for the two source configurations are presented in Section 4.

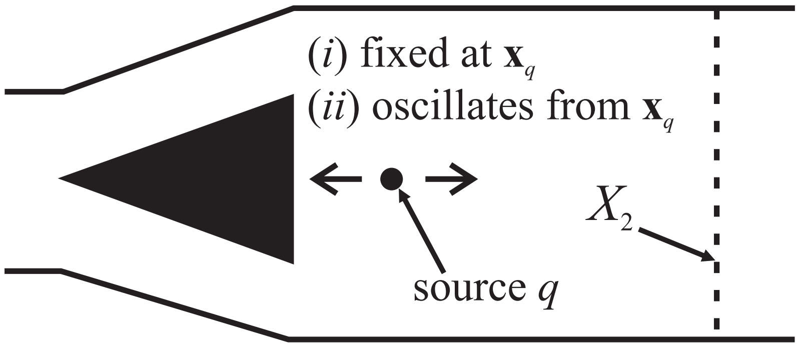

Figure 6: Depiction of the two chosen source configurations in the hydrodynamic region

4 Numerical Results

The dimensions of Rijke tube used in the LIMOUSINE project are used to obtain illustrative numerical results. It has respective upstream and downstream cross-sectional areas $\mathscr{A}_1 = 0.027$ m^2, $\mathscr{A}_2 = 0.052$ m^2. The flow enters the upstream section at room temperature and then increases by 200 K at X_2; the respective upstream and downstream temperatures are $\bar{T}_1 = 288$ K and $\bar{T}_2 = 488$ K. We assume an ideal gas and the ratios of the temperature and density are inversely related: $\bar{T}_1/\bar{T}_2 = 0.590$ and $\bar{\rho}_1/\bar{\rho}_2 = 1.695$. The respective speeds of sound in the upstream and downstream regions are $c_1 = 342$ m/s and $c_2 = 448$ m/s. The Rijke tube has length $L = 1.450$ m. Pressure nodes are located 0.014 m from the entrance and exit of the tube at locations $\ell_1 = -0.014$ m and $\ell_2 = 1.464$ m. The numerical results to the Schwarz-Christoffel transformation in Fig. 5 have shown that respective upstream and downstream interface locations $X_1 = 0.288$ m and $X_2 = 0.366$ m are sufficiently far from the burner to ensure the flow is one-dimensional. Further hydrodynamic calculations using eqn (4) have shown that $L_{eff} = 0.124$ m $= 1.6(X_2 - X_1)$. The source strength $q_o = 1$ m^2/s is fixed in each of the three cases discussed below.

Figure 7 depicts the time history of the time-domain Green's function. We limit the number of modes N in eqn (33) to 10 because experimental evidence shows that modes $n > 10$ are highly three-dimensional so they are not appropriate in the two-dimensional model. Experimental evidence also suggests that modes $n > 3$ are not significant in the unstable feedback mechanism. The time history is plotted at various positions x which range between X_2 and L. The Green's function depicted is typical for a summation of modes. The key feature to notice is the time delay observed; in each case, the time delay is approximately $(x - X_2)/c_2$.

Figure 8 shows the pressure distribution resulting from the stationary source of eqn (35) having source frequency $\omega_q = \omega_1$, where ω_n designates the n^{th} eigenfrequency. The figure shows the pressure at six evenly-distributed time-intervals ranging between $t = 0$ s and $t = 0.5$ s. Pressure is plotted against the non-dimensional axial position x/L ranging from the tube entrance $x/L = 0$ to the tube exit $x/L = 1$. In each of the three cases discussed, we present the pressure results similarly. The source is fixed at location $\mathbf{x}_q = (0.344, 0.006)$ m which is halfway between the downstream end of the flame holder and X_2.

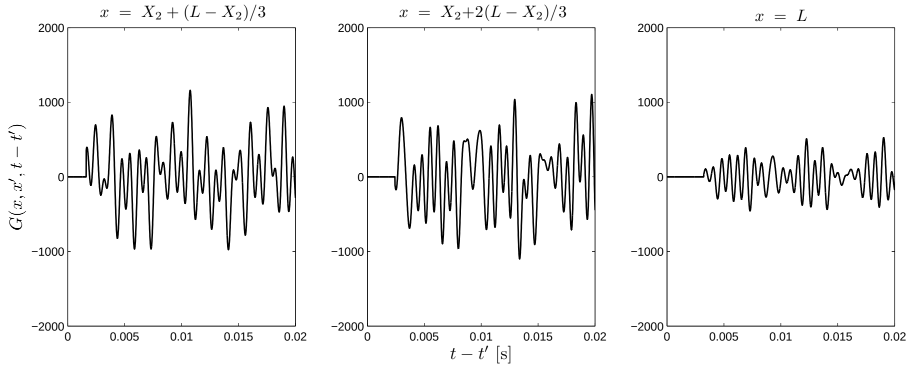

Figure 7: Green's function time history over $N = 10$ modes

Results show the single dominating frequency is $\omega_q = \omega_1 = 793.6\ \mathrm{s}^{-1}$ which is expected from eqn (36) and due to ω_1 being the only Rijke tube resonant frequency to be excited.

We also consider the effect of the source of eqn (37) having frequency ω_q oscillating axially at frequency $\omega_{q'}$. Figure 9 depicts the pressure distribution resulting from a source of frequency $\omega_q = \omega_2 = 1897\ \mathrm{s}^{-1}$ oscillating at frequency $\omega_{q'} = \omega_1$. The source oscillates axially between the downstream end of the burner and X_2 over a distance of $2|\mathbf{a}| = 0.044$ m and is centered at location $\mathbf{x}_q = (0.344, 0.006)$ m. We determine from eqn (38) that the dominating frequencies should be ω_q, $\omega_q + \omega_{q'}$ and $|\omega_q - \omega_{q'}|$; however, results show the only prevailing frequency to be ω_q, confirming that the effects of the oscillation frequency is small compared to the effect of the source frequency by a factor of 20.

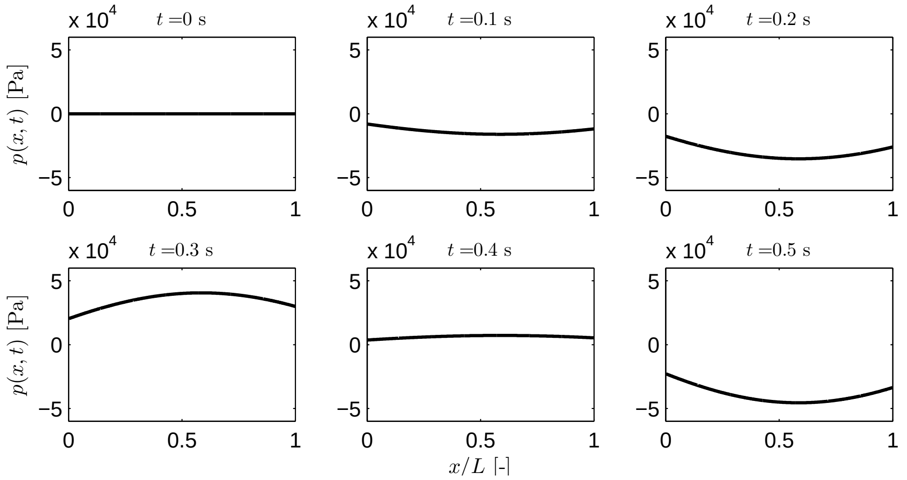

Figure 8: Pressure response from a source of frequency $\omega_q = \omega_1$

In order to show the effects of the oscillation frequency $\omega_{q'}$ separately from the source frequency ω_q, we assign the source frequency to a non-resonant frequency, say $\omega_q = (\omega_1 + \omega_2)/2 = 1345\ \mathrm{s}^{-1}$, and we assign the source oscillation frequency to the second resonant frequency $\omega_{q'} = \omega_2$. The resulting pressure response is depicted in Fig. 10. The pressure oscillations at frequency $\omega_{q'}$ are small in amplitude compared to those observed when the source frequency is resonant, as in Figs. 8-9.

5 Conclusion and outlook

The Green's function approach presented in this paper predicts the Rijke tube response to various sources configurations located in the hydrodynamic region. We choose the approach because we can

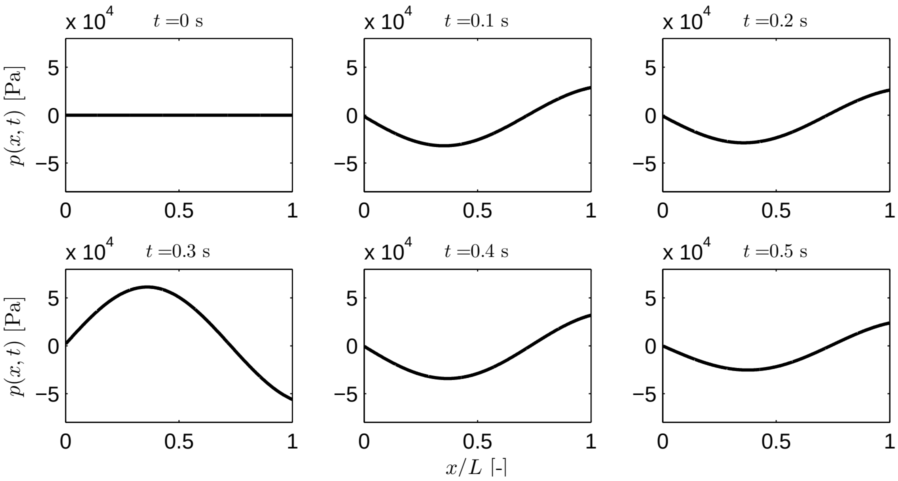

Figure 9: Pressure response from a translating source of frequency $\omega_q = \omega_2$, $\omega_{q'} = \omega_1$

extend it to account for other flame phenomena such as radiation losses.

Previous Rijke tube Green's function models use a linear approximation for the Green's function near the hydrodynamic region which cannot accurately account for the presence of large bodies such as the flame holder. We employ conformal mapping because it provides much more precise predictions, especially in the presence of large bodies. The Schwarz-Christoffel transformation allows us to model a source in the two-dimensional hydrodynamic region. Previous models were restricted to model sources in the hot acoustic region, far from the flame holder and the heat source. We expect that our model will better predict the stability of a particular Rijke tube geometry.

Our results show that for an oscillating point source in the hydrodynamic region it is the source frequency, not the oscillation frequency which is dominant. We would like to extend these results so they can account for the interaction between acoustics, combustion, and aerodynamics. For example, a vortex sheet forms from the downstream edge of the flame holder; we would like to use our results to model the effect due to the interaction of the vortices with the flame source.

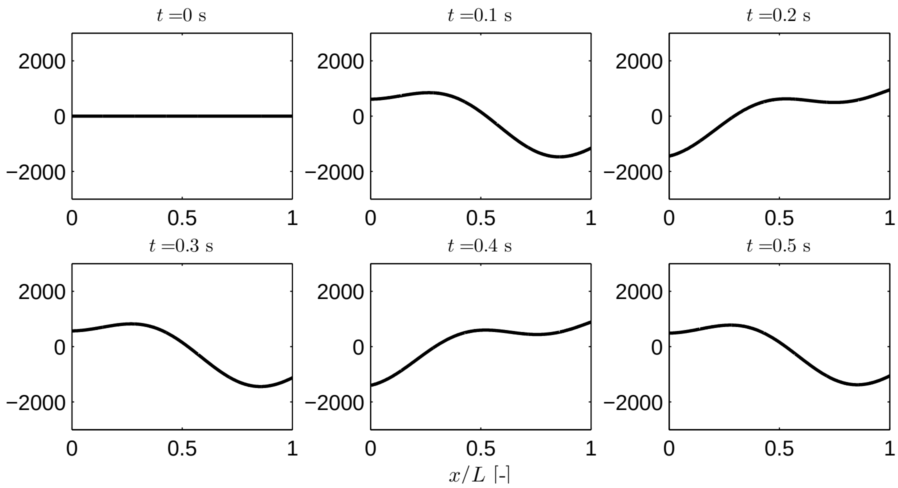

Figure 10: Pressure response from a translating source of frequency $\omega_q = (\omega_2 + \omega_1)/2$, $\omega_{q'} = \omega_2$

References

[1] M.A. Heckl and M.S. Howe. Stability analysis of the Rijke tube with a Green's function approach. *Journal of Sound and Vibration*, 305:672–688, 2007.

[2] M.S. Howe. *Theory of Vortex Sound*. Cambridge University Press, Cambridge, UK, 2003.

[3] M.S. Howe. *Hydrodynamics and Sound*. Cambridge University Press, Cambridge, UK, 2007.

[4] D. Howe. The application of numerical methods to the conformal transformation of polygonal boundaries. *Journal of the Institute of Mathematics and its Applications*, 12:125–136, 1973.

[5] F. Dias, A.R. Elcrat, and L.N. Trefethen. Ideal jet flow in two dimensions. *Journal of Fluid Mechanics*, 185:275–288, 1987.

[6] A.H. Stroud and D. Secrest. *Gaussian Quadrature Formulas*. Pretence-Hall, Englewood Cliffs, NJ, 1966.

[7] W.H. Press, B.P. Flannery, S.A. Teukolsky, and W.T. Vetterling. *Numerical Recipes*. Cambridge University Press, Cambridge, UK, 1986.

[8] M.S. Howe. *Acoustics of Fluid-Structure Interactions*. Cambridge University Press, Cambridge, England, 1998.

Acknowledgments

The authors would like to acknowledge scientific support from Professor Michael Howe as well as financial support from the European Commission.